Article

Colorimetric Detection and Killing of Bacteria by Enzyme-Instructed Self-Aggregation of Peptide-Modified Gold Nanoparticles

Dan Yin [1], Xiao Li [1], Xin Wang [2,*], Jin-Zhou Liu [1], Wen-Zhi She [1], Jiahui Liu [3,*], Jian Ling [1], Rong Sheng Li [1,*] and Qiue Cao [1]

[1] National Demonstration Center for Experimental Chemistry and Chemical Engineering Education (Yunnan University), School of Chemical Science and Engineering, Yunnan University, Kunming 650091, China; yindan@stu.ynu.edu.cn (D.Y.); lixiao_rwk0@stu.ynu.edu.cn (X.L.); 12021116015@mail.ynu.edu.cn (J.-Z.L.); swzhi21@mail.ynu.edu.cn (W.-Z.S.); lingjian@ynu.edu.cn (J.L.); qecao@ynu.edu.cn (Q.C.)

[2] Department of Orthopaedics, The Third Affiliated Hospital, Yunnan University of Chinese Medicine, Kunming 650051, China

[3] Institute of Biomedical Engineering, Kunming Medical University, Kunming 650500, China

*   Correspondence: wangxin@ynutcm.edu.cn (X.W.); liujiahui@kmmu.edu.cn (J.L.); lirong.sheng@ynu.edu.cn (R.S.L.)

Abstract: Bacterial infections seriously threaten human safety. Therefore, it is very important to develop a method for bacterial detection and treatment with rapid response, high sensitivity, and simple operation. A peptide CF_4KY^P (C, cysteine; F_4, phenylalanine tetrapeptide; K, lysine; Y^P, phosphorylated tyrosine) functionalized gold nanoparticle (AuNPs-CF_4KY^P) was synthesized for simultaneous detection and treatment of bacteria based on bacterial alkaline phosphatase (ALP). In solution, ALP can induce AuNPs-CF_4KY^P aggregation and produce significant color changes. After encountering bacteria, monodisperse AuNPs-CF_4KY^P can aggregate/assemble in situ on the surface of the bacterial membrane, change the color of the solution from wine red to grey, destroy the bacterial membrane structure, and induce the production of a large number of reactive oxygen species within the bacteria. The absorption change of AuNPs-CF_4KY^P solution has a good linear relationship with the number of bacteria. Furthermore, the aggregation of AuNPs-CF_4KY^P kills approximately 80% of *Salmonella typhimurium*. By combining enzyme-instructed peptide self-assembly technology and colorimetric analysis technology, we achieve rapid and sensitive colorimetric detection and killing of bacteria.

Keywords: gold nanoparticles; self-aggregation; bacteria detection; colorimetric detection; peptide

1. Introduction

Microbial infection poses a serious threat to human public health security with the growth of social population and environmental destruction. For example, *Salmonella typhimurium* (*S. typhimurium*), which is a food-borne pathogen [1], can induce typhoid fever, gastroenteritis, bacteremia, and other diseases [2,3]. According to statistics, the number of patients affected by *S. typhimurium* in China exceeds three million every year, accounting for 60% of food poisoning incidents [4]. Although many studies have been carried out on the design and construction of antimicrobial materials [5,6], the main technology is the use of chemical antimicrobials and antibiotics, which bring the side effects of bacterial resistance and secondary contamination [7]. In fact, many antimicrobial materials do not have the ability to simultaneously detect and kill bacteria. Moreover, the addition of bacterial detection to antimicrobial platforms is highly desirable for biomedical, environmental engineering, and clinical medicine [8,9]. Hence, materials that can detect and kill bacteria simultaneously are

critical for healthcare security research. However, little effort has been devoted to adding bacterial detection to the antimicrobial platform.

For bacterial detection, there are currently two main types of techniques [10]: One requires sample processing, including colony counting and polymerase chain reaction (PCR) [11], and the other requires large instruments, including biosensors based on aptamers, fluorescence [12,13], electrochemistry [14,15], and surface-enhanced Raman spectroscopy (SERS) [16–18]. However, these methods have certain disadvantages, such as the long time taken by plate counting, PCR is prone to false positive signals, and fluorescence and SERS are susceptible to interference from coexisting substances. Therefore, it is important to provide simple, fast, and accurate detection techniques and materials [19,20]. In addition, the detection method is of great importance, but the usual biosensors rely on the use of large instruments. In contrast, colorimetric detection has the advantage of on-site visualization and does not require large instruments [21,22]. Nanomaterials have a wide range of applications in biomedicine, organic, analytical, electrochemical, and other fields [23–25]. Gold nanoparticles (AuNPs) are ideal sensors [26] because they have high extinction coefficients and easy modification performance. The extinction coefficients are one thousand times larger than that of organic dyes. The size, shape, composition, and aggregate state of AuNPs determine the absorption frequency of the localized surface plasmon resonance (LSPR) [27]. AuNPs aggregates can be mediated by multiple strategies, resulting in the movement of LSPR bands and changes in visible color. As a commonly used colorimetric material, AuNPs are usually combined with biomolecules (such as peptides, proteins, and nucleic acids) for colorimetric detection [9,28,29].

At present, nanomaterials based on self-assembly peptides have been widely used in the detection and treatment of pathogenic bacteria. They are biological materials with certain functions and structures. Self-assembly is a process in which components spontaneously form an ordered structure without the intervention of external conditions [30], and the driving forces of self-assembly include intermolecular hydrogen bonds, van der Waals forces, electrostatic interactions, hydrophobic interactions, π-π stacking, etc. [31]. The peptide side chain contains different active functional groups (amino groups, carboxyl groups, and sulfhydryl groups), which are easy to artificially modify, and some functional groups can be connected to achieve various advantages, such as aggregation to enhance fluorescence emission, aggregation to enhance photoacoustic signal, in situ self-assembly induced mechanical effect [32–34]. Alkaline phosphatase (ALP) is an important hydrolase widely distributed in tissues and organs, such as the liver, bones, and kidneys of the human body [35]. It has good catalytic activity in the physiological environment, can catalyze the removal of phosphate groups in proteins, nucleic acids, and other small molecules, and is an important biomarker [36–38]. At present, there have been reports of using alkaline phosphatase-instructed peptide-functionalized nanomaterials for the killing of cancer cells [39–42], but there are very few reports of their use in the killing of bacteria. Therefore, this method is highly desirable for the detection and killing of Gram-negative bacteria with high ALP expression.

In this work, we constructed a strategy for simultaneous colorimetric detection and killing of bacteria by ALP-instructed self-aggregation of phosphorylated peptide-modified gold nanoparticles (AuNPs-CF$_4$KY^P). The AuNPs-CF$_4$KY^P is comprised of five individual functional motifs (Scheme 1A): (1) Gold nanoparticles (AuNPs) are signal motif and have different colors in the aggregated and dispersed states, which can be used for colorimetric analysis, (2) cysteine (C) is used to link to AuNPs because the sulfhydryl group of cysteine can form Au-S bonds with AuNPs, (3) phenylalanine tetrapeptide (F$_4$) is the reverse sequence of the β-sheet-forming peptide and provide sufficient hydrophobic interactions, (4) lysine (K) is a water-soluble amino acid and provide proper solubility for the probe, (5) phosphorylated tyrosine (Y^P) responds to ALP. The water-soluble AuNPs-CF$_4$KY^P can be dephosphorylated by bacterial ALP to form insoluble AuNPs-CF$_4$KY, which subsequently assembles into larger aggregates and causes a change in the color of the probe solution. The absorbance change of AuNPs-CF$_4$KY^P induced by bacteria has a good linear relationship

with the number of bacteria. According to the calculation, the detection limit is 7 CFU mL^{-1}, making bacterial quantification possible. Aggregation on the surface of bacteria destroys the structure of the bacterial membrane and produces large amounts of reactive oxygen species (ROS) inside the bacteria, which leads to the destruction of multiple-retained biosynthesis and metabolic pathways, leading to bacterial death, the bacterial killing rate can reach about 80%.
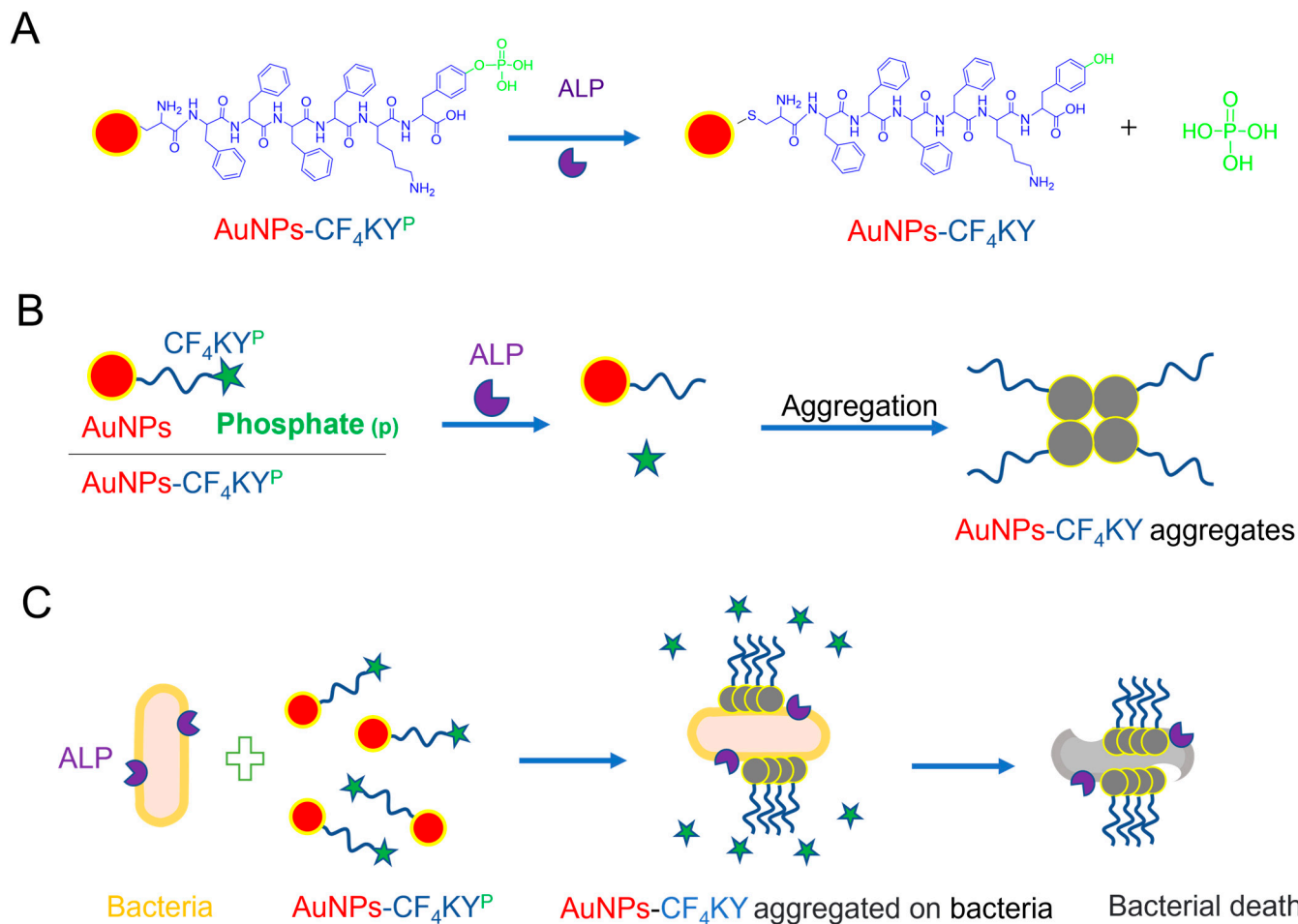
Scheme 1. Schematic illustration of colorimetric detection and killing of bacteria by AuNPs-CF$_4$KY^P. (**A**) The chemical structure of AuNPs-CF$_4$KY^P and the structure of ALP cleavage products AuNPs-CF$_4$KY. (**B**) The aggregation process of AuNPs-CF$_4$KY^P induced by ALP. (**C**) ALP cleavage products AuNPs-CF$_4$KY aggregate in situ on the surface of the bacteria, resulting in the color change of AuNPs-CF$_4$KY^P and bacterial death.

2. Experimental Section

2.1. Materials and Instruments

Gold acid chloride trihydrate (HAuCl$_4$·3H$_2$O, 99%), Trisodium citrate dihydrate (C$_6$H$_5$O$_7$Na$_3$, 99%), Sodium hydroxide (NaOH), and Hexafluoro-isopropanol (HFIP) were obtained from Titan Scientific Co., Ltd. (Shanghai, China). CF$_4$KY^P peptide was purchased from Shanghai Apeptide Co., Ltd. (Shanghai, China), Table S1, Figures S1 and S2). ALP was purchased from COOLABER SCIENCE and TECHNOLOGY Co., Ltd. (Beijing, China). The BBoxiProbeO13 bacterial ROS detection kit was obtained from BestBio Co., Ltd. (Shanghai, China). All reagents were used as received without further purification. Ultrapure water (18.25 MΩ) was used throughout the experiment.

UV–vis absorption spectra were acquired using a UV-2700 UV-vis spectrometer (Shimadzu, Tokyo, Japan). Dynamic light scattering (DLS) was performed at room temperature

using a Particle Size Analyzer (Brookhaven, New York, NY, USA). The ROS was measured using an F-7000 fluorescence spectrophotometer (Hitachi, Tokyo, Japan), and fluorescence microscopy was acquired using Olympus BX53 (manufacture, Tokyo, Japan).

2.2. Preparation and Characterization of the 13 nm AuNPs

The 13 nm AuNPs were synthesized using the sodium citrate reduction method according to the previously reported method [43]. To be specific, $HAuCl_4 \cdot 3H_2O$ (1 mM, 25 mL) was placed in a 100 mL round-bottomed flask. Next, heated and stirred to boiling reflux in an oil bath at 110 °C. Then, citric acid solution (38.8 mM, 2.5 mL) was quickly added and kept stirring for 20 min after it turned wine red. After stopping the heat, the solution was stirred to room temperature. Finally, the absorption spectra of AuNPs were recorded by a UV-vis spectrophotometer.

2.3. Preparation and Characterization of the AuNPs-CF_4KY^P

The CF_4KY^P peptide was designed by our group and synthesized by Shanghai Apeptide Co., Ltd. (Shanghai, China). The data of mass spectrometry and high-performance liquid chromatography of CF_4KY^P and mass spectrometry are shown in Figures S1 and S2. The CF_4KY^P was dissolved by HFIP (1 mg CF_4KY^P was dissolved by 500 μL HFIP). The processes of linking peptides to the surface of gold nanoparticles are as follows: step one, NaOH solution (0.15 M, 50 μL) was added into the test tube; step two, different amounts of CF_4KY^P solution (40, 20, 10, 0 μL) were added in the test tube, respectively, and mixed with NaOH solution; step three, AuNPs (1.5 mL) were added in the test tube, respectively, and incubated at room temperature for 2 h. Three kinds of probes (AuNPs-CF_4KY^P (20 μL CF_4KY^P), AuNPs-CF_4KY^P-1 (10 μL CF_4KY^P), AuNPs-CF_4KY^P-2 (40 μL CF_4KY^P)) were prepared for linking different numbers of CF_4KY^P molecules on the surface of AuNPs. Then, the properties of probes before and after adding ALP were tested by dynamic light scattering and UV-vis spectroscopy.

2.4. Transmission Electron Microscopy Characterization of AuNPs/AuNPs-CF_4KY^P

The morphology of AuNPs/AuNPs-CF_4KY^P was measured by transmission electron microscopy (TEM) (JEM-1200EX, JEOL, Tokyo, Japan). For TEM observation, carbon-coated 200-mesh copper grids (Beijing Zhongjingkeyi, Beijing, China) were freshly treated by glow discharge using a plasma cleaner. 10 μL of AuNPs/AuNPs-CF_4KY^P solution was dropped on the grid. After 30 s, the remaining liquid was blotted using the filter paper from the edge and air dried for 1 h before TEM observation.

2.5. Selectivity and Sensitivity of AuNPs-CF_4KY^P for ALP

For the selectivity study, the AuNPs-CF_4KY^P was incubated with alcohol dehydrogenase (ADH), lysozyme, trypsin, glucose oxidoreductase (GOD), malatedehydrogenase (MDH), and ALP, respectively, at a concentration of 3 $U \cdot mL^{-1}$ at 37 °C for 2 h. The absorption spectra were recorded by UV-vis spectroscopy. For the sensitivity study, serial concentrations of ALP from 2 to 4 $U \cdot mL^{-1}$ were incubated with AuNPs-CF_4KY^P at 37 °C for 3 h.

2.6. Selectivity and Sensitivity of AuNPs-CF_4KY^P for Bacterial ALP

For the selectivity study, *Escherichia coli* ATCC 25922 (*E. coli*), *Salmonella typhimurium* CGMCC1.1190 (*S. typhimurium*), *Klebsiella pneumoniae* ATCC 700603 (*K. pneumoniae*), *Acinetobacter baumannii* ATCC 19606 (*A. baumannii*), *Staphylococcus aureus* ATCC 23235 (*S. aureus*), and *Escherichia coli* DH-5α (*DH-5α*) were incubated, respectively, with AuNPs-CF_4KY^P at 37 °C for 3 h. For the sensitivity study, *S. typhimurium* suspensions with concentrations from 0 to 10^3 $CFU \cdot mL^{-1}$ were incubated with AuNPs-CF_4KY^P at 37 °C. The change in the color of the AuNPs-CF_4KY^P solution was taken with a mobile phone (OPPO PHA120), and the absorption spectra were recorded by UV-vis spectroscopy.

2.7. Antimicrobial Performance of AuNPs-CF$_4$KY^P

To study the mechanism of the AuNPs-CF$_4$KY^P against bacteria, *S. typhimurium* was incubated with the AuNPs-CF$_4$KY^P for 3 h and then tested by transmission electron microscopy (TEM) to observe the aggregation of AuNPs-CF$_4$KY^P on the bacterial surface and the changes of bacterial membrane structure. In addition, to verify whether there is reactive oxygen species (ROS) inside bacteria induced by aggregation of cleavage products AuNPs-CF$_4$KY, the bacterial ROS detection kit (BBoxiProbeO13) was used. The mechanism of ROS detection kit was that the O13 probe can be oxidized by ROS in bacterial cells to produce red fluorescent substances, and then the fluorescence intensity was observed by fluorescence spectrophotometer and fluorescence microscope. In order to observe the inhibition of *S. typhimurium* by AuNPs-CF$_4$KY^P, *S. typhimurium* was incubated with AuNPs-CF$_4$KY^P and sterile saline (control), respectively, at 37 °C for 3 h. After incubation, *S. typhimurium* was coated to the surface of LB medium with 1.5% agarose and cultured at 37 °C for one day. The bacterial inhibition rate was obtained by colony counting.

2.8. TEM Characterization of S. typhimurium

The bacteria morphology was measured by a TEM (HITACHI HT7800, Tokyo, Japan). For TEM observation, carbon-coated 200-mesh copper grids (Beijing Zhongjingkeyi) were freshly treated by glow discharge using a plasma cleaner. Ten microliters of pretreated *S. typhimurium* solution were dropped on the grid. After 1 min, the remaining liquid was blotted using the filter paper from the edge, and then 10 μL of uranyl acetate dihydrate (TED PELLA, 19481) was dropped on the grid. After 3 min, the remaining liquid was blotted using the filter paper from the edge and air dried for 1 h before TEM observation.

2.9. Statistical Analysis

All experiments were repeated three times. All data in this work are presented as mean values ± SD (Standard Deviation). Intergroup comparison was analyzed by Student's *t*-test (two-tailed). * means $p < 0.05$.

3. Results and Discussion

3.1. Preparation and Characterization of the 13 nm AuNPs and AuNPs-CF$_4$KY^P

The 13 nm AuNPs was synthesized using the sodium citrate reduction method. The AuNPs was wine red, UV–vis absorption was determined, and the maximum absorption peak was at 520 nm (Figure 1B). As shown in the TEM image (Figure 1A), the synthesized AuNPs have uniform morphology and size around 13 nm. The above experimental results indicate that 13 nm gold nanoparticles have been successfully synthesized. As shown in Scheme 1, AuNPs (13 nm) and CF$_4$KY^P molecules are connected through Au-S bonds because cysteine (C) in CF$_4$KY^P has the sulfhydryl group that can be linked to AuNPs. A large number of studies [44,45] have proved that Au and thiol group from cysteine can form Au-S bonds in an aqueous solution at room temperature. The formation of Au-S bonds can be verified by the redshift of the maximum absorption peak of the gold nanoparticles. In this work, the redshift of gold nanoparticles is about 5 nm after CF$_4$KY^P modification (Figure S3). To optimize the response performance of the probe to ALP, three probes (AuNPs-CF$_4$KY^P, AuNPs-CF$_4$KY^P-1, AuNPs-CF$_4$KY^P-2) were synthesized by adjusting the number of CF$_4$KY^P on the AuNPs. Then, UV–vis absorption and dynamic light scattering of three probes were measured at different times after incubating with ALP.
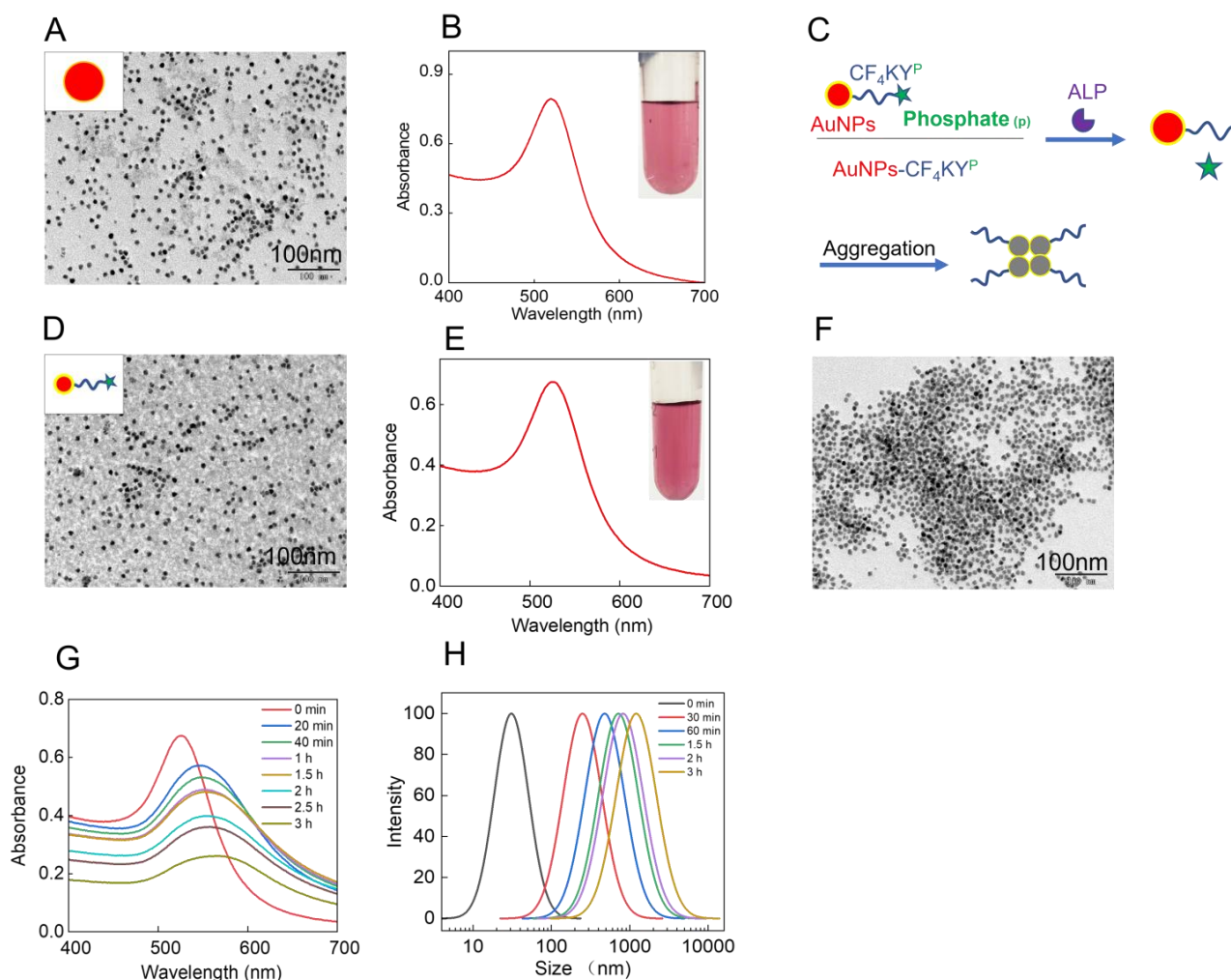
Figure 1. Preparation and characterization of AuNPs and AuNPs-CF_4KY^P. (**A**) TEM image and (**B**) UV–vis spectra of AuNPs. (**C**) Schematic illustration of the aggregation progress of AuNPs-CF_4KY^P after incubation with ALP. (**D**) TEM image of AuNPs-CF_4KY^P. (**E**) UV–vis spectra of AuNPs-CF_4KY^P. (**F**) TEM image of the ALP cleavage products AuNPs-CF_4KY. (**G**) UV–vis spectra and (**H**) hydrodynamic size profiles of AuNPs-CF_4KY^P before and after the addition of ALP. Experiments were repeated three times.

As shown in Figure S4A, it can be seen from the UV-vis absorption spectrum that the AuNPs-CF_4KY^P-1 did not respond significantly with ALP, which may be due to the low number of CF_4KY^P molecules on the surface of AuNPs, the hydrophobicity of the AuNPs-CF_4KY^P-1 was not significantly altered before and after ALP cleavage. It can be seen from the DLS results that the hydration particle size of AuNPs-CF_4KY^P-1 was about 30 nm before incubating with ALP. After AuNPs-CF_4KY^P-1 incubating with ALP for 3 h, the hydration particle size of AuNPs-CF_4KY^P-1 increased from 30 to 130 nm (Figure S4B), indicating that the aggregation of AuNPs-CF_4KY^P-1 is weak. The absorbance of AuNPs-CF_4KY^P (Figure 1G), AuNPs-CF_4KY^P-2 (Figure S4C) changed significantly after incubating with ALP for 3 h. The hydration particle size of the AuNPs-CF_4KY^P was about 30 nm before incubating with ALP, and the hydration particle size increased to 1300 nm after 3 h incubation with ALP (Figure 1H), indicating that the AuNPs-CF_4KY^P aggregation is significant after ALP incubation, which could be attributed to significant dephosphorylation of CF_4KY^P molecules on the surface of AuNPs. The hydration particle size of the AuNPs-CF_4KY^P-2 was also about 30 nm before incubating with ALP, and the hydration particle size reached about 1100 nm after 3 h incubation (Figure S4D). To achieve good ALP response performance and save CF_4KY^P, AuNPs-CF_4KY^P was used for subsequent experiments.

### 3.2. Response Ability of the AuNPs-CF$_4$KY^P to ALP

To study the selectivity of the AuNPs-CF$_4$KY^P to the enzyme, we incubated AuNPs-CF$_4$KY^P with ADH, lysozyme, trypsin, GOD, MDH, and ALP, respectively, for 2 h at 37 °C. The absorption changes were recorded with a UV-vis spectrophotometer. As shown in Figure 2A, only ALP caused significant changes in the absorbance of AuNPs-CF$_4$KY^P. The effect of other enzymes was negligible. In addition, noticeable color changes from wine red to gray in the solution can be observed by the naked eye when the AuNPs-CF$_4$KY^P was incubated with ALP (Figure 2B), which provides a possibility for the detection of bacterial ALP by colorimetry. The reason for the color change is that ALP dephosphorylates CF$_4$KY^P on the surface of AuNPs, forming a large number of hydrophobic AuNPs-CF$_4$KY, leading to the aggregation of AuNPs. The above results show that AuNPs-CF$_4$KY^P has good selectivity for ALP. The sensitivity of the AuNPs-CF$_4$KY^P to ALP was studied. Gradient concentrations of ALP ranging from 2 to 4 U·mL^{-1} were incubated with AuNPs-CF$_4$KY^P for 2 h at 37 °C. The change from wine red to gray in the solution (Figure S5B) was clearly observed by the naked eye, and the aggregates of AuNPs at the bottom of the test tube were clearly observed. As shown in Figure 2C,D, the standard curve shows that the absorbance of AuNPs-CF$_4$KY^P and the ALP concentration has a good linear relationship from 2 to 4 U·mL^{-1} with a correlation coefficient (R^2) of 0.999. These results show that the AuNPs-CF$_4$KY^P has good detection performance to ALP.
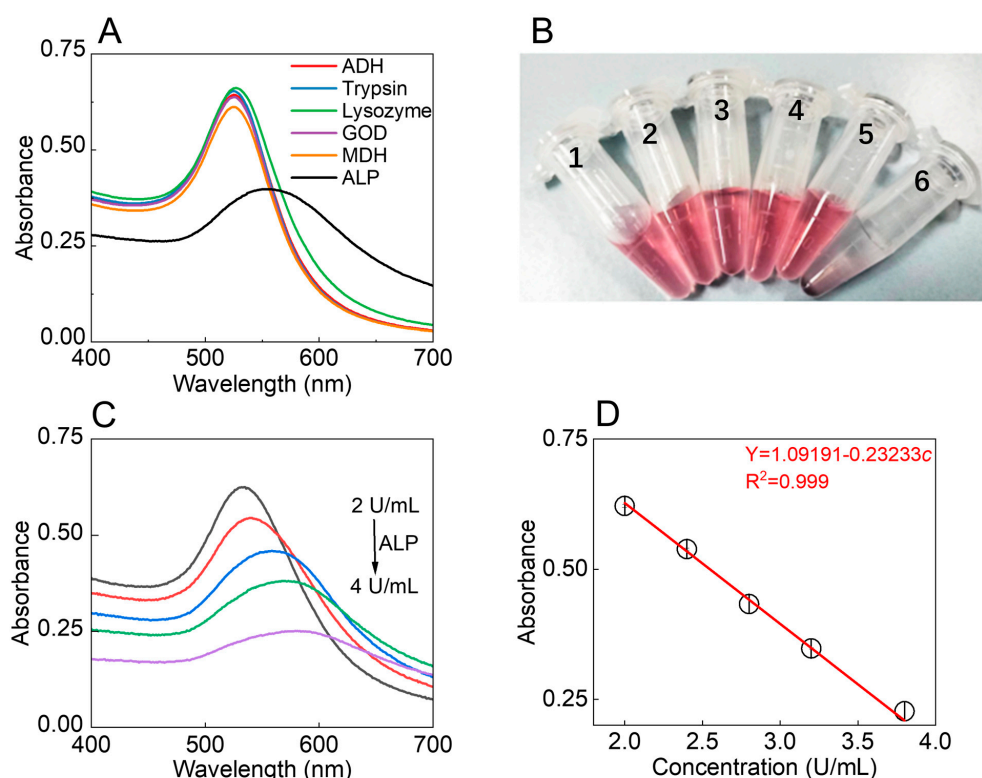
Figure 2. Selectivity and sensitivity studies of AuNPs-CF$_4$KY^P for ALP. (**A**) UV-vis spectra of AuNPs-CF$_4$KY^P incubated with different enzymes (ADH, lysozyme, trypsin, GOD, MDH, ALP). (**B**) The corresponding pictures of AuNPs-CF$_4$KY^P response to different enzymes. 1, ADH; 2, Trypsin; 3, Lysozyme; 4, GOD; 5, MDH; 6, ALP. (**C**) UV-vis spectra of AuNPs-CF$_4$KY^P at different concentrations of ALP (The concentrations of ALP corresponding to the absorption spectrum from top to bottom are 2.0, 2.4, 2.8, 3.2, 3.8 U/mL). (**D**) Linear relationship between the absorbance of AuNPs-CF$_4$KY^P (534 nm) and the ALP concentration. Experiments were repeated three times. (The midpoint of the circle represents the mean and the horizontal line represents the standard deviation). Data are presented as mean ± S.D. Error bars were obtained from three replicate experiments.

3.3. Response Ability of the AuNPs-CF$_4$KY^P to Bacterial ALP

For the selectivity study, *E. coli*, *S. typhimurium*, *K. pneumoniae*, *A. baumannii*, *S. aureus*, and *DH-5α* were incubated, respectively, with AuNPs-CF$_4$KY^P for 3 h at 37 °C, and the absorbance changes for different bacteria were recorded by a UV-vis spectrophotometer. As shown in Figure 3A,B, the absorbance of *S. typhimurium* group decreases significantly, while the absorbance change of other bacterial groups is almost negligible, indicating that the AuNPs-CF$_4$KY^P has good selectivity for *S. typhimurium*. In addition, the color change of the solution before and after adding bacteria to the AuNPs-CF$_4$KY^P can be observed by the naked eye, and the aggregation of particles can be clearly observed (Figure S6). The reason for the aggregation of the AuNPs-CF$_4$KY^P could be attributed to the highly expressed ALP by *S. typhimurium*. In practical applications, simple and rapid detection of *S. typhimurium* may be carried out by visually observing the color change of AuNPs-CF$_4$KY^P. The sensitivity of the AuNPs-CF$_4$KY^P for sensing *S. typhimurium* was determined. *S. typhimurium* suspensions with a concentration from 0 to 10^3 CFU·mL^{-1} were incubated with AuNPs-CF$_4$KY^P for 3 h at 37 °C. The absorption spectrum was recorded by a UV-vis spectrophotometer. As shown in Figure 3C,D, *S. typhimurium* was sensitively quantified with a good linear range from 10 to 10^3 CFU·mL^{-1} with a correlation coefficient (R^2) of 0.992. According to the calculation, the detection limit was 7 CFU·mL^{-1} (LOD = 3δ/k). The detection limit of the probe is relatively low compared with other reported bacterial colorimetric detection methods [10,21,46–62] (Supplementary Materials Table S2). These results indicate that the AuNPs-CF$_4$KY^P are selective and sensitive in response to *S. typhimurium*, and have a low detection limit, which has great application prospects in real life.
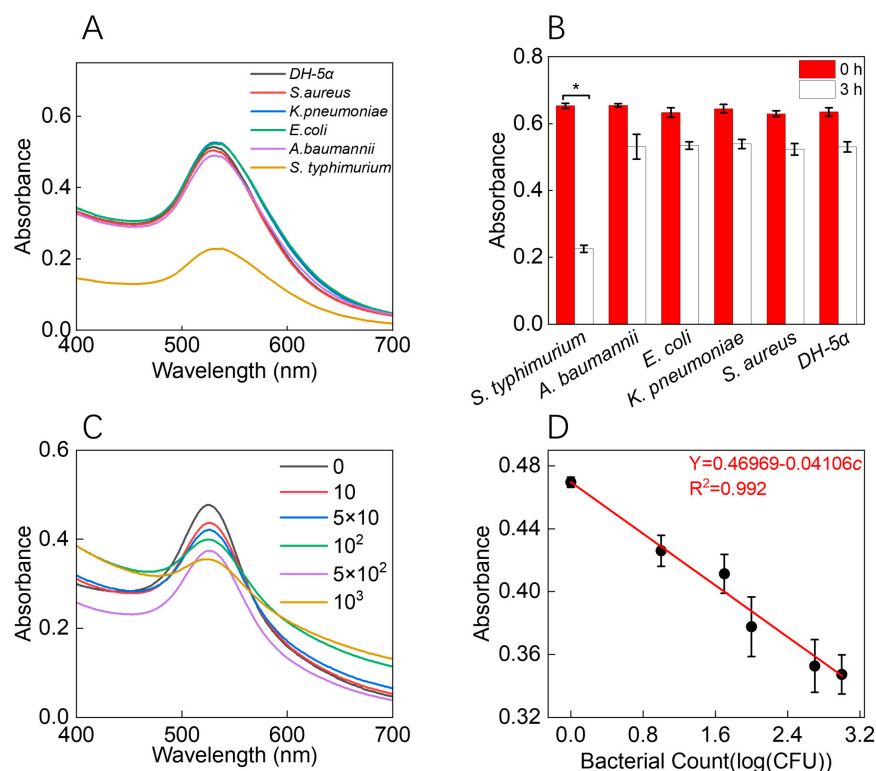

Figure 3. Specificity and sensitivity of the AuNPs-CF$_4$KY^P for bacteria. (**A**) UV-vis spectra and (**B**) the absorbance changes (530 nm) of the AuNPs-CF$_4$KY^P after incubating with different bacteria (*E. coli, S. typhimurium, K. pneumoniae, A. baumannii, S. aureus, and DH-5α*). (**C**) UV-vis spectra of AuNPs-CF$_4$KY^P after incubating with a different number of *S. typhimurium*. (**D**) Quantitative analysis of *S. typhimurium* according to the absorbance of AuNPs-CF$_4$KY^P at 530 nm. Experiments were repeated three times. Data in (**B,D**) are presented as mean ± S.D. Error bars were obtained from three replicate experiments. * means $p < 0.05$.

3.4. Antimicrobial Performance of AuNPs-CF$_4$KY^P

Based on the above results, we predict that a large number of ALP-cleavage products AuNPs-CF$_4$KY would accumulate on the bacterial surface, affecting the integrity of the bacterial membrane structure through the stress released during the aggregation process. In order to verify whether the AuNPs-CF$_4$KY^P has an inhibitory effect on bacteria, we used TEM imaging, fluorescence imaging, and colony-formation assay. According to the TEM images, we observed that gold nanoparticles accumulate on the surface of *S. typhimurium* and cause damage to the *S. typhimurium* membrane structure (Figure 4C,D). Furthermore, we found that AuNPs-CF$_4$KY aggregation induced a large number of ROS inside *S. typhimurium*. The ROS was stained by a commercial bacteria ROS kit (BBox-iProbeO13), which can generate strong red fluorescence after encountering ROS. According to the fluorescence microscopy images, we can see strong red fluorescence inside the *S. typhimurium* in the group that added the AuNPs-CF$_4$KY^P, while weak red fluorescence was observed in the control group (Figure 4B). According to the results of the fluorescence spectrophotometer, the fluorescence intensity of ROS in *S. typhimurium* incubated with AuNPs-CF$_4$KY^P increased by about seven times compared to the control group (Figure S8). ROS leads to intracellular redox homeostasis imbalance [63], which can destroy membrane proteins and various enzymes to prevent transmission of bacterial membrane-forming materials [64] and lead to bacteria physiological dysfunction and bacterial death. Based on the results of fluorescence and TEM, we speculated that gold nanoparticle aggregates on bacterial surfaces would effectively inhibit or kill *S. typhimurium*. Next, we tested the survival rate of *S. typhimurium* by incubating *S. typhimurium* with AuNPs-CF$_4$KY^P. To investigate the inhibitory efficiency of AuNPs-CF$_4$KY^P on *S. typhimurium*, *S. typhimurium* was incubated with the AuNPs-CF$_4$KY^P at 37 °C for 3 h, while the control group was incubated with sterile saline (three parallel experiments were performed for each group). After 3 h, *S. typhimurium* was coated on the surface of LB medium with 1.5% agarose and cultured at 37 °C for one day. The bacterial inhibition rate was obtained by colony counting. Approximately 80% of *S. typhimurium* was killed by the AuNPs-CF$_4$KY^P compared with the sterile saline group (Figures 4E,F and S7). These results indicated that the AuNPs-CF$_4$KY^P have a certain inhibitory effect on *S. typhimurium*, which provides a new approach for the simultaneous detection and killing of *S. typhimurium*. Currently, many materials are used for the detection or treatment of bacteria (Supplementary Materials Table S2), while few studies achieve both low detection limits and good antimicrobial performance. To date, the simultaneous detection and treatment of bacteria using gold nanoparticles is extremely rare. Since gold-based colorimetric detection has been widely used in the detection practice of pathogenic microorganisms, it is of great significance to realize gold-based colorimetric detection and treatment of pathogenic microorganisms at the same time. This strategy of enzyme-instructed self-aggregation of gold nanoparticles is promising for the simultaneous detection and killing of pathogenic microorganisms.
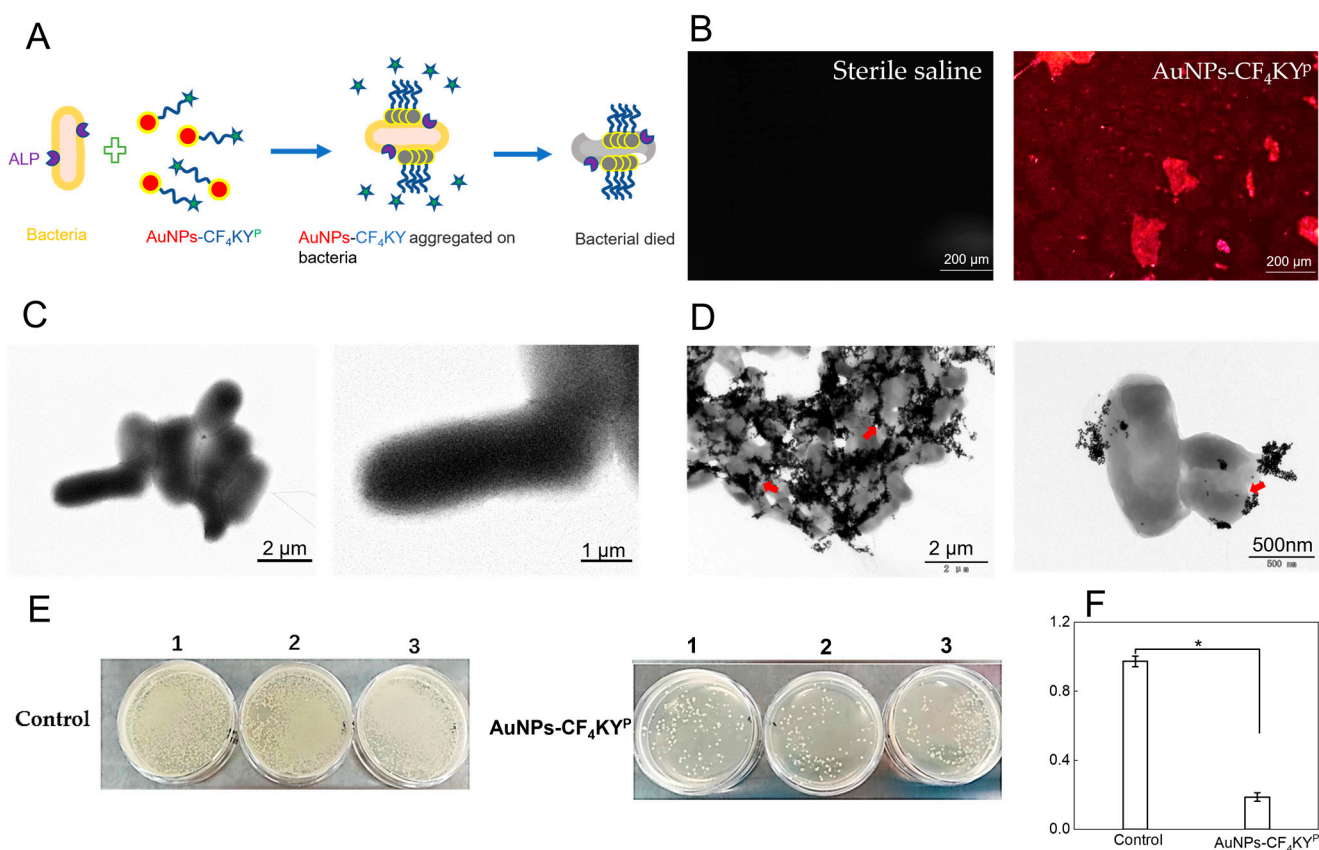
Figure 4. Inhibition of *S. typhimurium* by AuNPs-CF$_4$KY^P. (**A**) ALP cleavage products AuNPs-CF$_4$KY aggregate in situ on the surface of the bacteria. (**B**) ROS fluorescence images of *S. typhimurium* after incubating with AuNPs-CF$_4$KY^P or sterile saline. TEM images of *S. typhimurium* after incubating with (**C**) sterile saline or (**D**) AuNPs-CF$_4$KY^P. The red arrows indicate the disrupted outer membrane of the *S. typhimurium.* (**E**) Colony growth images of *S. typhimurium* after incubating with AuNPs-CF$_4$KY^P or sterile saline (control). (1, 2, and 3 represent three parallel experiments). (**F**) Statistical analysis of colony growth in E. Experiments were repeated three times. Data in (**B**,**D**) are presented as mean $\pm$ S.D. Error bars were obtained from three replicate experiments. * means $p < 0.05$.

4. Conclusions

In summary, based on the abnormally high expression of enzymes in bacteria, we designed a functional platform combining functionalized peptides with gold nanoparticles with low cost, simple operation, and intuitive signal for simultaneous visual detection and killing of bacteria. AuNPs-CF$_4$KY^P has good selectivity for *S. typhimurium*, and there is a good linear relationship between its absorbance change and the number of bacteria, which enables quantitative analysis. After encountering bacterial ALP, bacteria-induced cleavage products AuNPs-CF$_4$KY can accumulate on the surface of bacteria, destroy the bacterial membrane structure, lead to the production of ROS inside bacteria, and eventually induce bacterial death. AuNPs-CF$_4$KY^P has good bacterial killing performance, and its antibacterial efficiency can reach about 80%. This work achieves the simultaneous detection and treatment of *S. typhimurium*, which has certain potential application value. The combination of enzyme-indicated peptide self-assembly technology and colorimetric analysis technology used in this work provides a new strategy for simultaneously detection and killing bacteria.

References

1. Xie, M.; Chen, T.; Xin, X.; Cai, Z.; Dong, C.; Lei, B. Multiplex detection of foodborne pathogens by real-time loop-mediated isothermal amplification on a digital microfluidic chip. *Food Control* **2022**, *136*, 108824. [CrossRef]
2. Wang, B.; Liu, S.; Sui, Z.; Wang, J.; Wang, Y.; Gu, S. Rapid Flow Cytometric Detection of Single Viable Salmonella Cells in Milk Powder. *Foodborne Pathog. Dis.* **2020**, *17*, 447–458. [CrossRef] [PubMed]
3. Huang, F.; Xue, L.; Qi, W.; Cai, G.; Liu, Y.; Lin, J. An ultrasensitive impedance biosensor for Salmonella detection based on rotating high gradient magnetic separation and cascade reaction signal amplification. *Biosens. Bioelectron.* **2021**, *176*, 112921. [CrossRef] [PubMed]
4. Silva, S.; Teixeira, P.; Oliveira, R.; Azeredo, J. Adhesion to and viability of *Listeria monocytogenes* on food contact surfaces. *J. Food Prot.* **2008**, *71*, 1379–1385. [CrossRef]
5. Silver, L.L. Challenges of antibacterial discovery. *Clin. Microbiol. Rev.* **2011**, *24*, 71–109. [CrossRef] [PubMed]
6. Hajipour, M.J.; Fromm, K.M.; Ashkarran, A.A.; Jimenez de Aberasturi, D.; de Larramendi, I.R.; Rojo, T.; Serpooshan, V.; Parak, W.J.; Mahmoudi, M. Antibacterial properties of nanoparticles. *Trends Biotechnol.* **2012**, *30*, 499–511. [CrossRef]
7. Manzetti, S.; Ghisi, R. The environmental release and fate of antibiotics. *Mar. Pollut. Bull.* **2014**, *79*, 7–15. [CrossRef]
8. Mannoor, M.S.; Tao, H.; Clayton, J.D.; Sengupta, A.; Kaplan, D.L.; Naik, R.R.; Verma, N.; Omenetto, F.G.; McAlpine, M.C. Graphene-based wireless bacteria detection on tooth enamel. *Nat. Commun.* **2012**, *3*, 763. [CrossRef]

9. Disney, M.D.; Zheng, J.; Swager, T.M.; Seeberger, P.H. Detection of bacteria with carbohydrate-functionalized fluorescent polymers. *J. Am. Chem. Soc.* **2004**, *126*, 13343–13346. [CrossRef]

10. Ahmed, A.; Rushworth, J.V.; Hirst, N.A.; Millner, P.A. Biosensors for whole-cell bacterial detection. *Clin. Microbiol. Rev.* **2014**, *27*, 631–646. [CrossRef]

11. Jangampalli Adi, P.; Naidu, J.R.; Matcha, B. Multiplex quantification of *Escherichia coli*, *Salmonella typhi* and *Vibrio cholera* with three DNA targets in single reaction assay. *Microb. Pathog.* **2017**, *110*, 50–55. [CrossRef] [PubMed]

12. Fu, F.; Zhang, Y.; Li, L.; Wang, H.; Li, Q.; Tao, X.; Song, Y.; Song, E. Intracellular Pathogen Detection Based on Dual-Recognition Units Constructed Fluorescence Resonance Energy Transfer Nanoprobe. *Anal. Chem.* **2020**, *92*, 11462–11468. [CrossRef] [PubMed]

13. Yan, R.; Hu, Y.; Liu, F.; Wei, S.; Fang, D.; Shuhendler, A.J.; Liu, H.; Chen, H.-Y.; Ye, D. Activatable NIR Fluorescence/MRI Bimodal Probes for in Vivo Imaging by Enzyme-Mediated Fluorogenic Reaction and Self-Assembly. *J. Am. Chem. Soc.* **2019**, *141*, 10331–10341. [CrossRef] [PubMed]

14. Muniandy, S.; Teh, S.J.; Appaturi, J.N.; Thong, K.L.; Lai, C.W.; Ibrahim, F.; Leo, B.F. A reduced graphene oxide-titanium dioxide nanocomposite based electrochemical aptasensor for rapid and sensitive detection of *Salmonella enterica*. *Bioelectrochemistry* **2019**, *127*, 136–144. [CrossRef]

15. Appaturi, J.N.; Pulingam, T.; Thong, K.L.; Muniandy, S.; Ahmad, N.; Leo, B.F. Rapid and sensitive detection of Salmonella with reduced graphene oxide-carbon nanotube based electrochemical aptasensor. *Anal. Biochem.* **2020**, *589*, 113489. [CrossRef]

16. Zhou, S.; Lu, C.; Li, Y.; Xue, L.; Zhao, C.; Tian, G.; Bao, Y.; Tang, L.; Lin, J.; Zheng, J. Gold Nanobones Enhanced Ultrasensitive Surface-Enhanced Raman Scattering Aptasensor for Detecting *Escherichia coli* O157:H7. *ACS Sens.* **2020**, *5*, 588–596. [CrossRef]

17. Gao, X.; Yin, Y.; Wu, H.; Hao, Z.; Li, J.; Wang, S.; Liu, Y. Integrated SERS Platform for Reliable Detection and Photothermal Elimination of Bacteria in Whole Blood Samples. *Anal. Chem.* **2021**, *93*, 1569–1577. [CrossRef]

18. Liu, L.; Zhang, T.; Wu, Z.; Zhang, F.; Wang, Y.; Wang, X.; Zhang, Z.; Li, C.; Lv, X.; Chen, D.; et al. Universal Method for Label-Free Detection of Pathogens and Biomolecules by Surface-Enhanced Raman Spectroscopy Based on Gold Nanoparticles. *Anal. Chem.* **2023**, *95*, 4050–4058. [CrossRef]

19. Hu, J.; Tang, F.; Jiang, Y.Z.; Liu, C. Rapid screening and quantitative detection of Salmonella using a quantum dot nanobead-based biosensor. *Analyst* **2020**, *145*, 2184–2190. [CrossRef]

20. Li, Z.; Askim, J.R.; Suslick, K.S. The Optoelectronic Nose: Colorimetric and Fluorometric Sensor Arrays. *Chem. Rev.* **2019**, *119*, 231–292. [CrossRef]

21. Ma, X.; Song, L.; Zhou, N.; Xia, Y.; Wang, Z. A novel aptasensor for the colorimetric detection of *S. typhimurium* based on gold nanoparticles. *Int. J. Food Microbiol.* **2017**, *245*, 1–5. [CrossRef]

22. Wu, S.; Duan, N.; Qiu, Y.; Li, J.; Wang, Z. Colorimetric aptasensor for the detection of *Salmonella enterica* serovar typhimurium using $ZnFe_2O_4$-reduced graphene oxide nanostructures as an effective peroxidase mimetics. *Int. J. Food Microbiol.* **2017**, *261*, 42–48. [CrossRef]

23. Cheng, L.; Wang, X.; Gong, F.; Liu, T.; Liu, Z. 2D Nanomaterials for Cancer Theranostic Applications. *Adv. Mater.* **2020**, *32*, 1902333. [CrossRef]

24. Xu, J.; Hu, Y.; Wang, S.; Ma, X.; Guo, J. Nanomaterials in electrochemical cytosensors. *Analyst* **2020**, *145*, 2058–2069. [CrossRef]

25. Pirsa, S.; Alizadeh, N. Nanoporous Conducting Polypyrrole Gas Sensor Coupled to a Gas Chromatograph for Determination of Aromatic Hydrocarbons Using Dispersive Liquid-Liquid Microextraction Method. *IEEE Sens. J.* **2011**, *11*, 3400–3405. [CrossRef]

26. Lin, S.Y.; Wu, S.H.; Chen, C.H. A simple strategy for prompt visual sensing by gold nanoparticles: General applications of interparticle hydrogen bonds. *Angew. Chem. Int. Ed.* **2006**, *45*, 4948–4951. [CrossRef] [PubMed]

27. Li, R.S.; Zhang, H.Z.; Ling, J.; Huang, C.Z.; Wang, J. Plasmonic platforms for colorimetric sensing of cysteine. *Appl. Spectrosc. Rev.* **2016**, *51*, 129–147. [CrossRef]

28. Yang, S.; Yao, D.; Wang, Y.; Yang, W.; Zhang, B.; Wang, D. Enzyme-triggered self-assembly of gold nanoparticles for enhanced retention effects and photothermal therapy of prostate cancer. *Chem. Commun.* **2018**, *54*, 9841–9844. [CrossRef]

29. Zhao, W.; Chiuman, W.; Brook, M.A.; Li, Y. Simple and rapid colorimetric biosensors based on DNA aptamer and noncrosslinking gold nanoparticle aggregation. *ChemBioChem Eur. J. Chem. Biol.* **2007**, *8*, 727–731. [CrossRef] [PubMed]

30. Whitesides, G.M.; Grzybowski, B. Self-assembly at all scales. *Science* **2002**, *295*, 2418–2421. [CrossRef] [PubMed]

31. Zhang, S. Emerging biological materials through molecular self-assembly. *Biotechnol. Adv.* **2002**, *20*, 321–339. [CrossRef]

32. Song, S.; Qin, Y.; He, Y.; Huang, Q.; Fan, C.; Chen, H.Y. Functional nanoprobes for ultrasensitive detection of biomolecules. *Chem. Soc. Rev.* **2010**, *39*, 4234–4243. [CrossRef]

33. Li, H.; Huang, H.; Feng, J.J.; Luo, X.; Fang, K.M.; Wang, Z.G.; Wang, A.J. A polypeptide-mediated synthesis of green fluorescent gold nanoclusters for Fe^{3+} sensing and bioimaging. *J. Colloid Interface Sci.* **2017**, *506*, 386–392. [CrossRef] [PubMed]

34. Li, R.S.; Liu, J.; Shi, H.; Hu, P.P.; Wang, Y.; Gao, P.F.; Wang, J.; Jia, M.; Li, H.; Li, Y.F.; et al. Transformable Helical Self-Assembly for Cancerous Golgi Apparatus Disruption. *Nano Lett.* **2021**, *21*, 8455–8465. [CrossRef]

35. Lim, E.K.; Keem, J.O.; Yun, H.S.; Jung, J.; Chung, B.H. Smart nanoprobes for the detection of alkaline phosphatase activity during osteoblast differentiation. *Chem. Commun.* **2015**, *51*, 3270–3272. [CrossRef]

36. Kaliannan, K.; Hamarneh, S.R.; Economopoulos, K.P.; Nasrin Alam, S.; Moaven, O.; Patel, P.; Malo, N.S.; Ray, M.; Abtahi, S.M.; Muhammad, N.; et al. Intestinal alkaline phosphatase prevents metabolic syndrome in mice. *Proc. Natl. Acad. Sci. USA* **2013**, *110*, 7003–7008. [CrossRef] [PubMed]

37. Khan, A.R.; Awan, F.R.; Najam, S.S.; Islam, M.; Siddique, T.; Zain, M. Elevated serum level of human alkaline phosphatase in obesity. *J. Pak. Med. Assoc.* **2015**, *65*, 1182–1185.

38. Ooi, K.; Shiraki, K.; Morishita, Y.; Nobori, T. High-molecular intestinal alkaline phosphatase in chronic liver diseases. *J. Clin. Lab. Anal.* **2007**, *21*, 133–139. [CrossRef]

39. Zhou, J.; Du, X.; Berciu, C.; He, H.; Shi, J.; Nicastro, D.; Xu, B. Enzyme-Instructed Self-Assembly for Spatiotemporal Profiling of the Activities of Alkaline Phosphatases on Live Cells. *Chem* **2016**, *1*, 246–263. [CrossRef] [PubMed]

40. Tan, W.; Zhang, Q.; Wang, J.; Yi, M.; He, H.; Xu, B. Enzymatic Assemblies of Thiophosphopeptides Instantly Target Golgi Apparatus and Selectively Kill Cancer Cells. *Angew. Chem. Int. Ed.* **2021**, *60*, 12796–12801. [CrossRef] [PubMed]

41. Ding, Y.; Zheng, D.; Xie, L.; Zhang, X.; Zhang, Z.; Wang, L.; Hu, Z.W.; Yang, Z. Enzyme-Instructed Peptide Assembly Favored by Preorganization for Cancer Cell Membrane Engineering. *J. Am. Chem. Soc.* **2023**, *145*, 4366–4371. [CrossRef] [PubMed]

42. Liu, S.; Zhang, Q.; Shy, A.N.; Yi, M.; He, H.; Lu, S.; Xu, B. Enzymatically Forming Intranuclear Peptide Assemblies for Selectively Killing Human Induced Pluripotent Stem Cells. *J. Am. Chem. Soc.* **2021**, *143*, 15852–15862. [CrossRef] [PubMed]

43. Jiang, Y.; Shi, M.; Liu, Y.; Wan, S.; Cui, C.; Zhang, L.; Tan, W. Aptamer/AuNP Biosensor for Colorimetric Profiling of Exosomal Proteins. *Angew. Chem. Int. Ed.* **2017**, *56*, 11916–11920. [CrossRef] [PubMed]

44. Liu, Y.; Cao, Y.; Zhang, C.; Ye, C.; Bian, Q.; Cheng, X.; Xia, H.; Zheng, J.; Liu, H. A novel colorimetric method for H_2O_2 sensing and its application: Fe^{2+}-catalyzed H_2O_2 prevents aggregation of AuNPs by oxidizing cysteine (FeHOAuC). *Anal. Chim. Acta* **2022**, *1207*, 339840. [CrossRef]

45. Nie, H.-Y.; Romanovskaia, E.; Romanovski, V.; Hedberg, J.; Hedberg, Y.S. Detection of gold cysteine thiolate complexes on gold nanoparticles with time-of-flight secondary ion mass spectrometry. *Biointerphases* **2021**, *16*, 021005. [CrossRef] [PubMed]

46. Chen, F.; Chen, D.A.; Deng, T.; Li, J.S. Combination of Alkaline Phosphatase/Graphene Oxide Nanoconjugates and D-Glucose-6-Phosphate-Functionalized Gold Nanoparticles for the Rapid Colorimetric Assay of Pathogenic Bacteria. *Biosens. Bioelectron.* **2022**, *216*, 114611. [CrossRef]

47. Roh, S.G.; Robby, A.I.; Phuong, P.T.M.; In, I.; Park, S.Y. Photoluminescence-Tunable Fluorescent Carbon Dots-Deposited Silver Nanoparticle for Detection and Killing of Bacteria. *Mater. Sci. Eng. C.* **2019**, *97*, 613–623. [CrossRef]

48. Zhang, X.; Ren, C.H.; Hu, F.; Gao, Y.; Wang, Z.Y.; Li, H.Q.; Liu, J.F.; Liu, B.; Yang, C.H. Detection of Bacterial Alkaline Phosphatase Activity by Enzymatic in Situ Self-Assembly of the Aiegen-Peptide Conjugate. *Anal. Chem.* **2020**, *92*, 5185–5190. [CrossRef] [PubMed]

49. Wang, L.; Wu, X.; Hu, H.; Huang, Y.; Yang, X.; Wang, Q.; Chen, X. Improving the Detection Limit of Salmonella Colorimetry Using Long Ssdna of Asymmetric-Pcr and Non-Functionalized Aunps. *Anal. Biochem.* **2021**, *626*, 114229. [CrossRef] [PubMed]

50. Yang, H.; Xiao, M.; Lai, W.; Wan, Y.; Li, L.; Pei, H. Stochastic DNA Dual-Walkers for Ultrafast Colorimetric Bacteria Detection. *Anal. Chem.* **2020**, *92*, 4990–4995. [CrossRef]

51. Le, T.N.; Tran, T.D.; Kim, M.I. A Convenient Colorimetric Bacteria Detection Method Utilizing Chitosan-Coated Magnetic Nanoparticles. *Nanomaterials* **2020**, *10*, 92. [CrossRef] [PubMed]

52. Kang, E.B.; Mazrad, Z.a.I.; Robby, A.I.; In, I.; Park, S.Y. Alkaline Phosphatase-Responsive Fluorescent Polymer Probe Coated Surface for Colorimetric Bacteria Detection. *Eur. Polym. J.* **2018**, *105*, 217–225. [CrossRef]

53. Wang, K.-Y.; Bu, S.-J.; Ju, C.-J.; Li, C.-T.; Li, Z.-Y.; Han, Y.; Ma, C.-Y.; Wang, C.-Y.; Hao, Z.; Liu, W.-S.; et al. Hemin-Incorporated Nanoflowers as Enzyme Mimics for Colorimetric Detection of Foodborne Pathogenic Bacteria. *Bioorg. Med. Chem. Lett.* **2018**, *28*, 3802–3807. [CrossRef] [PubMed]

54. Wang, J.; Cao, Y.; Li, Z.; Dong, M.; Dou, W.; Xu, X.; He, S. Bridge-DNA Synthesis Triggered by an Allosteric Aptamer for the Colorimetric Detection of Pathogenic Bacteria. *Anal. Methods* **2023**, *15*, 275–283. [CrossRef] [PubMed]

55. Huang, J.; Sun, J.; Warden, A.R.; Ding, X. Colorimetric and Photographic Detection of Bacteria in Drinking Water by Using 4-Mercaptophenylboronic Acid Functionalized Aunps. *Food Control* **2020**, *108*, 106885. [CrossRef]

56. Liu, Y.; Zhao, C.; Zhao, W.; Zhang, H.; Yao, S.; Shi, Y.; Li, J.; Wang, J. Multi-Functional Mno2-Doped Fe3o4 Nanoparticles as an Artificial Enzyme for the Colorimetric Detection of Bacteria. *Anal. Bioanal. Chem.* **2020**, *412*, 3135–3140. [CrossRef]

57. Wang, C.; Gao, X.; Wang, S.; Liu, Y. A Smartphone-Integrated Paper Sensing System for Fluorescent and Colorimetric Dual-Channel Detection of Foodborne Pathogenic Bacteria. *Anal. Bioanal. Chem.* **2020**, *412*, 611–620. [CrossRef]

58. Chen, Q.M.; Gao, R.; Jia, L. Enhancement of the Peroxidase-Like Activity of Aptamers Modified Gold Nanoclusters by Bacteria for Colorimetric Detection of Salmonella Typhimurium. *Talanta* **2021**, *221*, 121476. [CrossRef]

59. Bahadoran, A.; Jabarabadi, M.K.; Mahmood, Z.H.; Bokov, D.; Janani, B.J.; Fakhri, A. Quick and Sensitive Colorimetric Detection of Amino Acid with Functionalized-Silver/Copper Nanoparticles in the Presence of Cross Linker, and Bacteria Detection by Using DNA-Template Nanoparticles as Peroxidase Activity. *Spectrochim. Acta A* **2022**, *268*, 120636. [CrossRef]

60. Bagheri Pebdeni, A.; Hosseini, M. Fast and Selective Whole Cell Detection of Staphylococcus Aureus Bacteria in Food Samples by Paper Based Colorimetric Nanobiosensor Using Peroxidase-Like Catalytic Activity of DNA-Au/Pt Bimetallic Nanoclusters. *Microchem. J.* **2020**, *159*, 105475. [CrossRef]

61. Sun, J.; Huang, J.; Li, Y.; Lv, J.; Ding, X. A Simple and Rapid Colorimetric Bacteria Detection Method Based on Bacterial Inhibition of Glucose Oxidase-Catalyzed Reaction. *Talanta* **2019**, *197*, 304–309. [CrossRef] [PubMed]

62. Verdoodt, N.; Basso, C.R.; Rossi, B.F.; Pedrosa, V.A. Development of a Rapid and Sensitive Immunosensor for the Detection of Bacteria. *Food Chem.* **2017**, *221*, 1792–1796. [CrossRef] [PubMed]

63. Zhou, Z.; Li, B.; Liu, X.; Li, Z.; Zhu, S.; Liang, Y.; Cui, Z.; Wu, S. Recent Progress in Photocatalytic Antibacterial. *ACS Appl. Bio Mater.* **2021**, *4*, 3909–3936. [CrossRef] [PubMed]
64. Wang, Y.; Zhao, Y.; Wu, J.; Li, M.; Tan, J.; Fu, W.; Tang, H.; Zhang, P. Negatively Charged Sulfur Quantum Dots for Treatment of Drug-Resistant Pathogenic Bacterial Infections. *Nano Lett.* **2021**, *21*, 9433–9441. [CrossRef] [PubMed]